JACS
JOURNAL OF THE AMERICAN CHEMICAL SOCIETY
Communication
pubs.acs.org/JACS

Histidine–Iridium(III) Coordination-Based Peptide Luminogenic Cyclization and Cyclo-RGD Peptides for Cancer-Cell Targeting

Xiaochuan Ma,[†,‡] Junli Jia,[†] Rui Cao,[†] Xiaobo Wang,[†] and Hao Fei*[,†]

[†]CAS Key Laboratory of Nano-Bio Interface, Suzhou Key Laboratory for Nanotheranostics, Division of Nanobiomedicine, Suzhou Institute of Nano-Tech and Nano-Bionics, Chinese Academy of Sciences, Suzhou 215123, China

[‡]Graduate School of the Chinese Academy of Sciences, Beijing 100049, China

Supporting Information

ABSTRACT: In the field of peptide drug discovery, structural constraining and fluorescent labeling are two sought-after techniques important for both basic research and pharmaceutical development. In this work, we describe an easy-to-use approach for simultaneous peptide cyclization and luminescent labeling based on iridium(III)–histidine coordination (Ir–HH cyclization). Using a series of model peptides with histidine flanking each terminus, the binding activity and reaction kinetics of Ir–HH cyclization of different ring sizes were characterized. In the series, Ir–HA$_n$H (n = 2, 3) with moderate ring sizes provides appropriate flexibility and proper distance between histidines for cyclic formation, which leads to the best binding affinity and structural stability in physiological conditions, as compared to other Ir–HH-cyclized peptides with smaller (n = 0, 1) or larger (n = 4, 5) ring sizes. Ir–HRGDH, an Ir–HH-cyclized peptide containing integrin targeting motif Arg-Gly-Asp (RGD), showed better targeting affinity than its linear form and enhanced membrane permeability in comparison with fluorescein-labeled cyclic RGDyK peptide. Cell death inducing peptide KLA-linked Ir–HRGDH (Ir–HRGDH–KLA) showed dramatically enhanced cytotoxicity and high selectivity for cancer cells versus noncancer cells. These data demonstrate that the method conveniently combines structural constraining of peptides with luminescent imaging capabilities, which facilitates functional and intracellular characterization of potential peptide-based drug leads, thus introducing a new tool to meet emerging needs in medicinal research.

Peptides, as natural ingredient of biological systems, occupy a chemical middle space between small compounds and large biologics for drug design and discovery. However, short peptides are often unsuitable for direct pharmaceutical application due to their inherent conformational flexibility.[1,2] To circumvent these limitations, various strategies have been applied for peptide macrocyclization to improve stability, mimic natural protein structures, and enhance functional performance.[3−6] Some recent works highlight the stabilization of specific α-helical peptides to interfere protein–protein interactions using the methods of hydrocarbon stapling[7,8] or hydrogen bond surrogates.[9] Other studies on RGD,[10] MSH,[11] HAV,[12] and conotoxin[13] peptides, linked the free ends of the peptides via disulfide bridges or amide condensation methods to create looped structures. In addition to these covalent-bond-based methods, coordination-based approaches may provide alternative strategies for structural constraining of peptides. Many previous studies have explored the effects of metal/nonmetal elements in stabilizing peptide structures.[14−18] In addition to a structure constraining role, coordination can also confer advantageous features. For example, rhenium and technetium have been used to cyclize melanotropin peptide analogues while simultaneously providing imaging and radiotherapeutic modalities.[19] As previously reported, the coordination between transition metal iridium(III) complex and histidines can be used for protein staining and cell imaging.[20,21] The combination of structural constraining and phosphorescent labeling properties may provide additional novel features that are beneficial for biomedicinal research and warrant further exploration.

We report herein an easy-to-use and versatile method for peptide luminogenic cyclization through the coordination of Ir(III) complex (Bis(2-phenylpyridine-C^2,N)-bis(aquo)iridium(III)trifluoromethanesulfonate) (Scheme S1, Supporting Information (SI)) to the imidazole group of the histidine side chain, a process that is referred to as Ir–HH cyclization in the remainder of this article (Figure 1A). We first synthesized a series of model linear peptides with increasing numbers of alanines placed between two histidines (Ac–HA$_n$H, n = 0, 1, 2, 3, 4, or 5) (Figure 1B). These peptides all produced strong green phosphorescence after 2 h of incubation with the Ir(III) complex (Figure S1, SI). The in-solution binding stoichiometry between Ir(III) complex and Ac–HA$_n$H peptides was determined by Job plot method.[22] In the assay, reaction mixtures were prepared with different Ir/peptide ratios when the total concentrations of Ir and peptide were maintained at 0.1 mM. The maximum emission intensity was achieved when the molar fraction of the peptide was 0.5, as shown in Figure 1C, indicating a 1:1 binding stoichiometry. This binding stoichiometry was further confirmed by mass spectrometry, when excessive peptides were mixed with Ir(III) complex and the only mass species detected in each reaction besides unreacted peptides were the bimolecular binding products (Figures S2–S7, SI). As the N-termini of these peptides were acetylated, it ensures the participation of both histidine residues in Ir(III) coordination (reaction model 2 in Scheme S1, SI, as determined in ref 21), thus leading to the formation of Ir–HH cyclo-peptides complexes.

Received: November 12, 2014
Published: December 8, 2014

ACS Publications © 2014 American Chemical Society

dx.doi.org/10.1021/ja511656q | J. Am. Chem. Soc. 2014, 136, 17734–17737

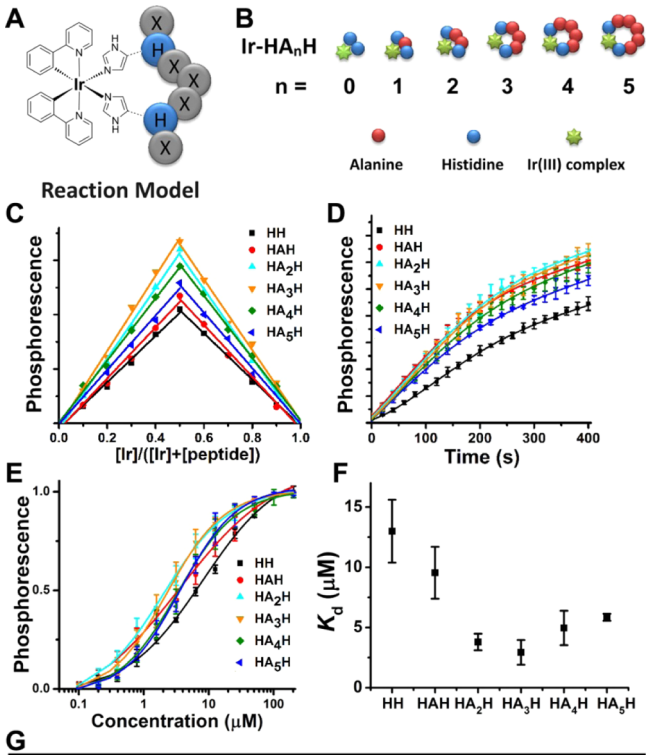

G

	HH	HAH	HA_2H	HA_3H	HA_4H	HA_5H
EC_{50} (μM)	8.07 ±1.06	3.87 ±0.78	2.07 ±0.55	2.53 ±0.76	3.4 ±0.87	3.7 ±0.46
K_d (μM)	13.00 ±2.61	9.54 ±2.15	3.80 ±0.68	2.93 ±1.03	4.96 ±1.43	5.84 ±0.29

Figure 1. Characterization of Ir−HH cyclization of peptides of different ring sizes. (A) Schematic illustration of Ir−HH-based peptide cyclization. Each circle denotes an amino acid residue. H denotes histidine; X denotes any amino acid except histidine. (B) A series of model Ir−HH-cyclized peptides with an increasing number of alanines placed between the two histidines. (C) Job plot of the Ir−HA$_n$H (n = 0−5) complexes in PBS. (D) Initial time courses (0−400 s) of the reaction of Ir(III) complex (12.5 μM) with peptides (12.5 μM) of different ring sizes. (E−G) Specific interaction of Ir(III) complex with different peptides. (E) The equilibrium binding assays of Ir(III) complex (0.5 μM) and peptides at the indicated concentrations (0.1−200 μM). EC_{50} values were determined by nonlinear regression analysis of dose−response curves by using Prism software 5.0 (GraphPad). (F) Plot of equilibrium dissociation constants (K_d). (G) Specific values of EC_{50} and K_d.

The progress of the cyclization reaction can be readily monitored by the increase in the phosphorescence intensity of the resulting end-products. The initial time course of the reaction showed that peptides with alanine(s) inserted between two histidines all exhibited fast initial rates of reaction with the Ir(III) complex, while Ac−HH reacted comparatively slower (Figure 1D). This luminogenic reaction allows a simple estimation of Ir−peptide binding equilibriums (EC_{50}) by a solution-phase phosphorescence titration assay, in which Ir(III) complex (0.5 μM) interacts with Ac−HA$_n$H (n = 0−5) peptides over a concentration range of 0.1 to 200 μM (Figure 1E). In the series, Ac−HH exhibited weaker binding to Ir(III) than all other peptides with alanine insertions (Figure 1G). To measure more accurately the reaction kinetic parameters and dissect the differences in the peptide series, a large excess of peptides was incubated with Ir(III) complex to allow for pseudo-first-order reactions. Association kinetic experiments were performed with multiple peptide concentrations, and the data were globally fit to the association kinetic model to derive a single best-fit estimate by using Prism software 5.0 (GraphPad) for k_{on}, k_{off}, and K_d (Figure S8 and Table S1, SI). Figure 1F illustrates a graphical comparison of K_ds among peptide rings of different sizes. In the peptide series, Ac−HH had both the lowest K_d and initial reaction rate. The steric hindrance from the rigid amide plane of the adjacent trans-configured histidine side chains of this peptide probably limited the reaction rate. Ir−HA$_n$H (n = 2, 3) with moderate ring sizes provides appropriate flexibility and proper distance between histidines for cyclic formation, which predicts superior affinity and stability in comparison with other Ir−HH-cyclized peptides with smaller (n = 1) or larger (n = 4, 5) ring sizes. EC_{50} and K_d values for binding are shown in Figure 1G.

To further assess the ring stability for in vitro or in vivo applications, experiments were conducted with potential coordination competitors under physiological conditions, e.g., divalent cationic ions or histidine-rich albumin at their serum concentrations, or glutathione at its cytoplasmic concentration. Co-incubation with Zn(II), Cu(II), Ca(II), or Mg(II) indicated poor competitive capacity for Ir(III)−peptides of different ring sizes (Figure S9A, SI). Co-incubation of bovine serum albumin (BSA) with Ir(III)−peptides followed by SDS-PAGE indicated that BSA barely competed with peptide−Ir(III) at its cytoplasmic concentration (0.5 mM), and negligible BSA−Ir was produced (Figure S9B, SI). When Ir−HH cyclic peptides were incubated with 5 mM glutathione, their luminescent intensity decreased slowly over 10 h. Ir−HA$_n$H (n = 2, 3) retained more than 80% of its initial phosphorescence, suggesting better stability under reducing conditions than smaller or larger rings of Ir−HA$_n$H (n = 1, 4, or 5, with over 65% phosphorescence retained) (Figure S9C, SI). Taken together, these observations indicate sufficient stability of Ir−HH-cyclized peptides under simulated physiological conditions.

The results described above show that medium ring sizes with 2−3 amino acid insertions have the highest reaction rate and stability. To demonstrate this luminescent cyclization technique, a selected example is the well-studied tripeptide sequence RGD. As a targeting motif, RGD has been applied to mediate specific binding with integrin $\alpha_v\beta_3$ receptor, especially in tumor optical imaging,[23] anticancer peptides,[24,25] or drug delivery systems.[26] The cyclic forms of peptides containing RGD have been reported to be more competitive than linear forms in both cell adhesion activity and targeting specificity.[10]

The structural formula of Ir−HRGDH is shown in Figure 2A. Ir−HRGDH was purified by using high performance liquid chromatography (Figure S10, SI), and its molecular weight was confirmed by mass spectra (Figure S11, SI). The phosphorescence profiles of Ir−HRGDH and the control linear peptide RGDHH (labeled with the Ir(III) complex) are shown in Figure S12, SI.

To confirm RGD in its cyclized form performs better than its linear form in $\alpha_v\beta_3$ integrin positive cell (human lung cancer cell A549) uptake, a linear RGD peptide-labeled with Ir(III) complex (RGDHH−Ir) was used as a control. Both peptides (10 μM) were incubated with A549 cells, and images were captured by using confocal laser scanning microscopy. Ir−HRGDH-treated cells showed extensive punctate phosphorescence distribution in the cytoplasm, whereas cells incubated with RGDHH-Ir showed only sporadic staining (Figure 2B). Further quantitative assays measuring residual phosphorescence in the culture medium after incubation showed that coincubation of Ir−HRGDH with A549 cells resulted in obvious reduction of the phosphorescence in the

dx.doi.org/10.1021/ja511656q | J. Am. Chem. Soc. 2014, 136, 17734−17737

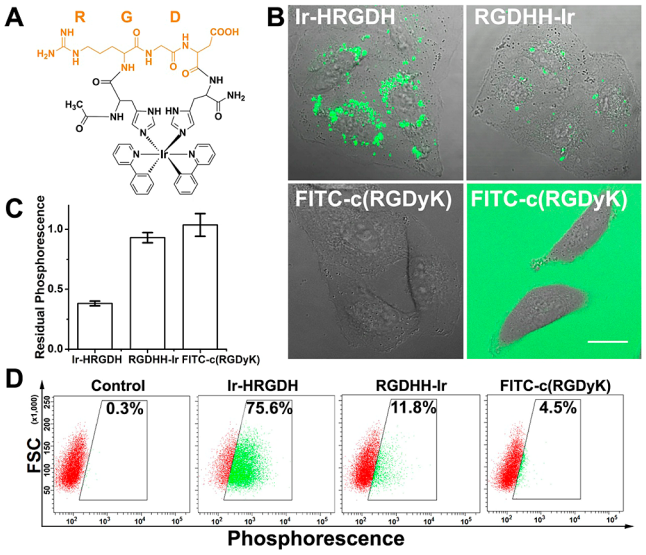

Figure 2. Better cellular uptake of Ir−HRGDH. (A) Structure illustration of Ir−HRGDH. (B−D) Cell uptake behavior study by using (B) confocal laser scanning microscopy, (C) the residual phosphorescence assay, and (D) flow cytometry in A549 cells incubated with Ir−HRGDH (10 μM, λ_{ex} = 405 nm), RGDHH−Ir (10 μM, λ_{ex} = 405 nm), or FITC−c(RGDyK) (10 μM, λ_{ex} = 488 nm) for 24 h at 37 °C. The scale bar represents 20 μm.

medium, while almost 90% of the total RGDHH−Ir phosphorescence was retained in the culture medium (Figure 2C). Using the same culture conditions, flow cytometry studies were also performed, and the results are presented as a forward scatter (FSC) versus fluorescence dot plot. An obvious increase in the percentage (75.6%) of green phosphorescent spherical cells was observed after Ir−HRGDH incubation. In contrast, RGDHH−Ir showed lower association with A549 cells (11.8%), indicating poor cell uptake (Figure 2D). In another control experiment, we examined whether Ir−HRGDH showed α_v integrin-dependent cell uptake in the MCF-7 breast cancer cell line, which expresses $\alpha_v\beta_3$ integrin at low levels.[29] As expected, Ir−HRGDH exhibited little internalization in MCF-7 cells (Figure S13, SI). Taking advantage of spontaneous luminescent labeling, these imaging assays and quantitative analyses confirmed that the RGD sequence and its Ir−HH-cyclized form provide the specificity and affinity required to mediate attachment and entry into $\alpha_v\beta_3$ integrin-expressing cancer cells.

Next, we compared the luminescent cyclization approach with a traditional head-to-tail cyclic RGD peptide (c(RGDyK)). FITC-labeled c(RGDyK) (10 μM) was incubated with A549 cells for 24 h. For better contrast, confocal images were taken before (right) and after (left) replacing the culture medium with FITC−c(RGDyK) (Figure 2B). In FITC−c(RGDyK)-treated cells, very little fluorescence was observed, indicating poor uptake efficiency. Results of the residual phosphorescence assay and flow cytometry studies for cells were both in agreement with the confocal imaging results (Figure 2B−D). Besides the minor conformational differences in the two ring structures, it is possible that this dramatic difference in uptake was due to the positively charged and arene-rich Ir(III) complex being more lipophilic than conventional organic fluorescent dyes, such as FITC and Alexa Fluor dyes.[21,27,28]

Additional functional peptide segments can be further tethered to Ir−HH cyclized peptides. Here, to evaluate its anticancer efficacy, the Ir−HRGDH peptide was C-terminally extended with the cationic peptide KLA ($(KLAKLAK)_2$), the cytotoxicity of which has been greatly limited by its poor uptake efficiency. MTT assay was used to assess the cytotoxicity of a series of peptide constructs toward A549 cells (Figure 3A). Ir−

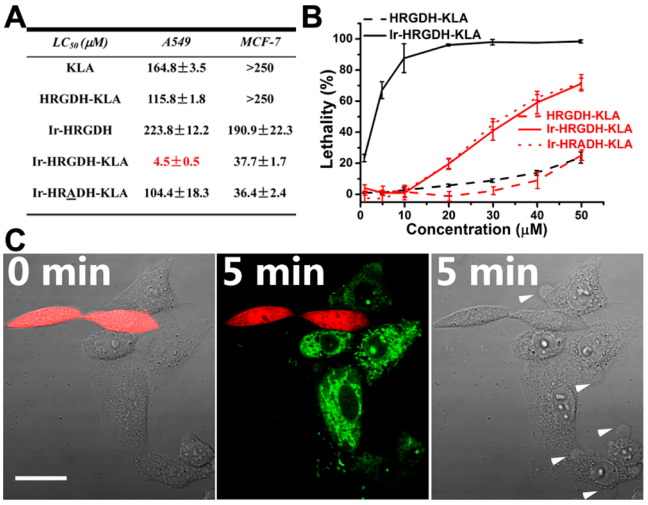

LC_{50} (μM)	A549	MCF-7
KLA	164.8±3.5	>250
HRGDH-KLA	115.8±1.8	>250
Ir-HRGDH	223.8±12.2	190.9±22.3
Ir-HRGDH-KLA	4.5±0.5	37.7±1.7
Ir-HRADH-KLA	104.4±18.3	36.4±2.4

Figure 3. Enhanced and selective cytotoxicity of Ir−HRGDH−KLA. (A) Table of the LC_{50} values of peptide compounds in A549 and MCF-7 cells. (B) Dose−response lethality curve of Ir−HRGDH−KLA, HRGDH−KLA, and/or Ir−HRADH−KLA in A549 (black lines) or MCF-7 (red lines) cells. Data represent the mean ± standard deviation of three independent experiments. (C) Time-lapse confocal images of cocultured live A549 and HLF cells incubated with Ir−HRGDH−KLA (10 μM). A549 cells showed Ir−HRGDH−KLA uptake (green) and morphological changes (blebbing, white arrowheads), whereas HLF cells expressing RFP (red) did not show Ir−HRGDH−KLA uptake or morphological change. The scale bar represents 20 μm.

HRGDH-guided KLA (Ir−HRGDH−KLA) had an LC_{50} (4.5 μM) reduced by 2 orders of magnitude in comparison with free KLA. For comparison, Ir−HRGDH alone or uncyclized HRGDH−KLA showed no significant cytotoxicity, with LC_{50} values of 223.8 and 115.8 μM, respectively. Another control peptide, with the glycine of RGD replaced by an alanine (Ir−HRADH−KLA), also showed a higher LC_{50} (104.4 μM), stressing the integrin targeting specificity of the RGD sequence.

We also evaluated Ir−HRGDH−KLA cytotoxicity in MCF-7 cells. In contrast to A549 cells, cyclization promoted cytotoxicity much more weakly in MCF-7 cells, as shown in Figure 3A,B. The increased cytotoxicity caused by cyclization was most likely due to the improved overall membrane permeability of Ir−HRGDH−KLA, rather than to the RGD motif itself. As a further investigation, Ir−HRADH−KLA was next tested in MCF-7 cells and, as expected, displayed a similar trend of cytotoxicity as that of Ir−HRGDH−KLA. These results highlight the cyclo-RGD-dependent targeting and cell killing effect in A549 cells.

In another model, we showed that the green phosphorescence of the cyclized peptide allows direct visualization of its selective targeting behavior. Here, noncancer human lung fibroblast (HLF) cells expressing transfected red fluorescent protein (RFP) were cocultured with A549 cells for 24 h. Confocal images of live cells (Figure 3C) showed that when Ir−HRGDH−KLA (10 μM) was added to the coculture, selective and rapid uptake and cytoplasmic dispersion of the peptide occurred only to polygonal-shaped A549 cells. In 5 min, membrane blebbing (white arrowheads) and nuclear condensation, typical character-

dx.doi.org/10.1021/ja511656q | J. Am. Chem. Soc. 2014, 136, 17734−17737

istics of apoptosis, specifically occurred to A549 cells. In stark contrast, no green luminescent signal or any morphological signs of apoptosis were observed in the smaller, spindle-shaped HLF cells (red). Thus, in the above example, we demonstrated that Ir−HH-cyclized functional peptides can be further derivatized for applications such as anticancer therapeutic development. Combined with the phosphorescence from Ir−HH cyclization, this method allows convenient and convincing assessment of the cell selectivity of therapeutic peptide compounds.

In summary, our work describes a novel luminogenic peptide cyclization approach utilizing histidine−iridium(III) complex coordination chemistry, which displays several interesting features, including a highly efficient and easy-to-use cyclization procedure, luminescent end products for instant monitoring or molecular tracing, and cell membrane permeability for intracellular delivery. Simultaneous luminescent labeling along with conformational constraining may provide a platform similar to the tetracysteine tag-based technique for studies of peptide−protein interactions.[30] It may also be applied to constrain recently uncovered loop-structured peptide motifs involved in protein−protein interaction[31] and allow for rapid affinity/activity screening with target molecules. The Ir−HH cyclization method reported here should enrich the rapidly growing toolbox for future peptide structure−function studies.

■ ASSOCIATED CONTENT

Supporting Information

Experimental details, Ir−HH cyclization and characterization results, binding reaction model and kinetics results, and results for the stability of Ir−HH-cyclized peptides in physiological conditions. This material is available free of charge via the Internet at http://pubs.acs.org.

■ AUTHOR INFORMATION

Corresponding Author

*hfei2008@sinano.ac.cn

Notes

The authors declare no competing financial interest.

■ ACKNOWLEDGMENTS

We thank SunaTech Inc. for providing iridium complexes. We are grateful to Dr. Ming Zhou, lab members, and SINANO microscopy facility for invaluable discussions and technical supports. This work was supported by Natural Science Foundation of China Grants 31170777, 21302213, and 30900341.

■ REFERENCES

(1) Vlieghe, P.; Lisowski, V.; Martinez, J.; Khrestchatisky, M. *Drug Discovery Today* **2010**, *15*, 40.
(2) Craik, D. J.; Fairlie, D. P.; Liras, S.; Price, D. *Chem. Biol. Drug Des.* **2013**, *81*, 136.
(3) Demmer, O.; Frank, A. O.; Kessler, H. In *Peptide and Protein Design for Biopharmaceutical Applications*; Jensen, K. J., Ed.; Wiley: New York, 2009; Vol. *1*, pp 133−176.
(4) Craik, D. J.; Swedberg, J. E.; Mylne, J. S.; Cemazar, M. *Expert Opin. Drug Discovery* **2012**, *7*, 179.
(5) Dharanipragada, R. *Future Med. Chem.* **2013**, *5*, 831.
(6) Roxin, Á.; Zheng, G. *Future Med. Chem.* **2012**, *4*, 1601.
(7) Verdine, G. L.; Hilinski, G. J. *Drug Discovery Today* **2012**, *9*, e41.
(8) Walensky, L. D.; Kung, A. L.; Escher, I.; Malia, T. J.; Barbuto, S.; Wright, R. D.; Wagner, G.; Verdine, G. L.; Korsmeyer, S. J. *Science* **2004**, *305*, 1466.
(9) Henchey, L. K.; Jochim, A. L.; Arora, P. S. *Curr. Opin. Chem. Biol.* **2008**, *12*, 692.
(10) Fani, M.; Psimadas, D.; Zikos, C.; Xanthopoulos, S.; Loudos, G. K.; Bouziotis, P.; Varvarigou, A. D. *Anticancer Res.* **2006**, *26*, 431.
(11) Chen, J.; Cheng, Z.; Owen, N. K.; Hoffman, T. J.; Miao, Y.; Jurisson, S. S.; Quinn, T. P. *J. Nucl. Med.* **2001**, *42*, 1847.
(12) Williams, E. *J. Biol. Chem.* **2000**, *275*, 4007.
(13) Xu, S.; Li, H.; Shao, X.; Fan, C.; Ericksen, B.; Liu, J.; Chi, C.; Wang, C. *J. Med. Chem.* **2012**, *55*, 6881.
(14) Cline, D. J.; Thorpe, C.; Schneider, J. P. *J. Am. Chem. Soc.* **2003**, *125*, 2923.
(15) Ghadiri, M. R.; Choi, C. *J. Am. Chem. Soc.* **1990**, *112*, 1630.
(16) Kelso, M. J.; Beyer, R. L.; Hoang, H. N.; Lakdawala, A. S.; Snyder, J. P.; Oliver, W. V.; Robertson, T. A.; Appleton, T. G.; Fairlie, D. P. *J. Am. Chem. Soc.* **2004**, *126*, 4828.
(17) Ma, M. T.; Hoang, H. N.; Scully, C. C. G.; Appleton, T. G.; Fairlie, D. P. *J. Am. Chem. Soc.* **2009**, *131*, 4505.
(18) Micklitsch, C. M.; Knerr, P. J.; Branco, M. C.; Nagarkar, R.; Pochan, D. J.; Schneider, J. P. *Angew. Chem.* **2011**, *123*, 1615.
(19) Giblin, M. F.; Wang, N.; Hoffman, T. J.; Jurisson, S. S.; Quinn, T. P. *Proc. Natl. Acad. Sci. U.S.A.* **1998**, *95*, 12814.
(20) Ma, D. L.; Wong, W. L.; Chung, W. H.; Chan, F. Y.; So, P. K.; Lai, T. S.; Zhou, Z. Y.; Leung, Y. C.; Wong, K. Y. *Angew. Chem.* **2008**, *120*, 3795. 028.
(21) Wang, X.; Jia, J.; Huang, Z.; Zhou, M.; Fei, H. *Chem.—Eur. J.* **2011**, *17*, 8.
(22) Renny, J. S.; Tomasevich, L. L.; Tallmadge, E. H.; Collum, D. B. *Angew. Chem., Int. Ed.* **2013**, *52*, 11998.
(23) Ye, Y.; Chen, X. *Theranostics* **2011**, *1*, 102.
(24) Dufort, S.; Sancey, L.; Hurbin, A.; Foillard, S.; Boturyn, D.; Dumy, P.; Coll, J. L. J. *Drug Targeting* **2011**, *19*, 582.
(25) Ellerby, H. M.; Arap, W.; Ellerby, L. M.; Kain, R.; Andrusiak, R.; Del Rio, G.; Krajewski, S.; Lombardo, C. R.; Rao, R.; Ruoslahti, E.; Bredesen, D. E.; Pasqualini, R. *Nat. Med.* **1999**, *5*, 1032.
(26) Ruoslahti, E.; Bhatia, S. N.; Sailor, M. J. *J. Cell Biol.* **2010**, *188*, 759.
(27) Cao, R.; Jia, J.; Ma, X.; Zhou, M.; Fei, H. *J. Med. Chem.* **2013**, *56*, 3636.
(28) Jones, A. T.; Sayers, E. J. *J. Controlled Release* **2012**, *161*, 582.
(29) Lin, R. Y.; Dayananda, K.; Chen, T. J.; Chen, C. Y.; Liu, G. C.; Lin, K. L.; Wang, Y. M. *Contrast Media Mol. Imaging* **2012**, *7*, 7.
(30) Luedtke, N. W.; Dexter, R. J.; Fried, D. B.; Schepartz, A. *Nat. Chem. Biol.* **2007**, *3*, 779.
(31) Gavenonis, J.; Sheneman, B. A.; Siegert, T. R.; Eshelman, M. R.; Kritzer, J. A. *Nat. Chem. Biol.* **2014**, *10*, 716.

■ NOTE ADDED AFTER ASAP PUBLICATION

Figure 3 was replaced December 11, 2014.